nature genetics

Mutations in the HECT domain of *NEDD4L* lead to AKT–mTOR pathway deregulation and cause periventricular nodular heterotopia

Loïc Broix[1–5,22], Hélène Jagline[1–4,22], Ekaterina L Ivanova[1–4], Stéphane Schmucker[1–4], Nathalie Drouot[1–4], Jill Clayton-Smith[6], Alistair T Pagnamenta[7], Kay A Metcalfe[6], Bertrand Isidor[8], Ulrike Walther Louvier[9], Annapurna Poduri[10], Jenny C Taylor[7], Peggy Tilly[1–4], Karine Poirier[5], Yoann Saillour[5], Nicolas Lebrun[5], Tristan Stemmelen[1–4], Gabrielle Rudolf[1–4], Giuseppe Muraca[5], Benjamin Saintpierre[5], Adrienne Elmorjani[5], Deciphering Developmental Disorders study[11], Martin Moïse[12], Nathalie Bednarek Weirauch[13], Renzo Guerrini[14], Anne Boland[15], Robert Olaso[15], Cecile Masson[16], Ratna Tripathy[17], David Keays[17], Cherif Beldjord[18], Laurent Nguyen[12], Juliette Godin[1–4], Usha Kini[19], Patrick Nischké[16], Jean-François Deleuze[15], Nadia Bahi-Buisson[20], Izabela Sumara[1–4], Maria-Victoria Hinckelmann[1–4] & Jamel Chelly[1–4,21]

Neurodevelopmental disorders with periventricular nodular heterotopia (PNH) are etiologically heterogeneous, and their genetic causes remain in many cases unknown. Here we show that missense mutations in *NEDD4L* mapping to the HECT domain of the encoded E3 ubiquitin ligase lead to PNH associated with toe syndactyly, cleft palate and neurodevelopmental delay. Cellular and expression data showed sensitivity of PNH-associated mutants to proteasome degradation. Moreover, an *in utero* electroporation approach showed that PNH-related mutants and excess wild-type NEDD4L affect neurogenesis, neuronal positioning and terminal translocation. Further investigations, including rapamycin-based experiments, found differential deregulation of pathways involved. Excess wild-type NEDD4L leads to disruption of Dab1 and mTORC1 pathways, while PNH-related mutations are associated with deregulation of mTORC1 and AKT activities. Altogether, these data provide insights into the critical role of NEDD4L in the regulation of mTOR pathways and their contributions in cortical development.

Development of the human cerebral cortex requires coordinated spatial and temporal regulation of interdependent developmental processes that include proliferation, migration and layering, as well as differentiation of distinct neuronal populations[1,2]. Disruption of any of these processes can result in a wide range of developmental disorders. Many of these disorders are classified within the group of malformations of cortical development (MCD) that includes lissencephaly, pachygyria, polymicrogyria (PMG), microcephaly and PNH[3–5]. MCD are often associated with severe intellectual disability and epilepsy, and their evolving classification is based on the developmental process thought to be affected first in combination with the underlying disrupted genes and biological pathways[3].

Within the group of MCD associated with neuronal migration abnormalities, PNH represents about 31% of MCD (R.G., unpublished data). Anatomically, PNH is characterized by bilateral ectopic nodules of gray matter lining the lateral ventricles. Clinical presentations in patients with PNH are heterogeneous, although seizures and learning difficulties are the most common clinical features[5].

So far, mutations in the X-linked *FLNA* gene (filamin A)[6], encoding a widely expressed 280-kDa actin-binding phosphoprotein, account

[1]Institut de Génétique et de Biologie Moléculaire et Cellulaire, Illkirch, France. [2]CNRS U7104, Illkirch, France. [3]INSERM U964, Illkirch, France. [4]Université de Strasbourg, Illkirch, France. [5]Institut Cochin, INSERM U1016, CNRS U8104, Paris Descartes University, Paris, France. [6]Manchester Centre for Genomic Medicine, Central Manchester University Hospitals NHS Trust, Manchester Academic Health Science Centre, Manchester, UK. [7]NIHR Biomedical Research Centre, Wellcome Trust Centre for Human Genetics, University of Oxford, Oxford, UK. [8]Service de Génétique Médicale, University Hospital of Nantes, Nantes, France. [9]Unité de Neuropédiatrie et d'Epileptologie Infantile, University Hospital of Montpellier, Montpellier, France. [10]Epilepsy Genetics Program, Division of Epilepsy and Clinical Neurophysiology, Department of Neurology, Boston Children's Hospital, Boston, Massachusetts, USA. [11]A list of members and affiliations appears at http://dx.doi.org/10.1101/049056. [12]Grappe Interdisciplinaire de Génoprotéomique Appliquée-Neurosciences, University of Liège, Liège, Belgium. [13]Hôpital Maison Blanche, University Hospital of Reims, Reims, France. [14]Paediatric Neurology Unit, A. Meyer Children's Hospital, University of Florence, Florence, Italy. [15]Centre National de Génotypage, Institut de Génomique, CEA, Evry, France. [16]Institut Imagine, Bioinformatics Platform, Paris Descartes University, Paris, France. [17]Institute of Molecular Pathology, Vienna, Austria. [18]Laboratoire de Biochimie et Génétique Moléculaire, Hôpital Cochin, Paris, France. [19]Department of Clinical Genetics, Oxford University Hospitals NHS Trust, Oxford, UK. [20]Institut Imagine, INSERM U1163, Paris Descartes University, Hôpital Necker–Enfants Malades, Paris, France. [21]Service de Diagnostic Génétique, Hôpital Civil de Strasbourg, Hôpitaux Universitaires de Strasbourg, Strasbourg, France. [22]These authors contributed equally to this work. Correspondence should be addressed to J.C. (chelly@igbmc.fr).

Received 1 April; accepted 24 August; published online 3 October 2016; doi:10.1038/ng.3676

for about 50% of bilateral PNH and the associated Ehler–Danlos conditions affecting mostly females[7]. Compelling studies suggested that *FLNA*-related PNH results from the combination of defects affecting the polarized radial glia scaffold and its adhesion to the neuroependymal membrane, neural progenitor proliferation and neuronal migration[8–10]. Other mechanisms contributing to PNH development were proposed following the identification of rare familial forms of PNH associated with recessive mutations in *ARFGEF2*, which encodes the ADP–ribosylation factor guanine exchange factor 2 (GEF2)[11]. Finally, other genetic forms of PNH have been mapped through array comparative genomic hybridization (aCGH) studies, but only one potential causal gene, *C6orf70* (*ERMARD*) located at 6q27, has been identified[12].

Here we provide evidence implicating the E3 ubiquitin ligase gene *NEDD4L* in the development of PNH. We report the identification of missense mutations in *NEDD4L* in patients with PNH, bilateral syndactyly, cleft palate and neurodevelopmental delay. We further show that PNH-related NEDD4L mutants disrupt neurodevelopmental processes, likely through dysregulation of the mTOR and AKT signaling pathways.

RESULTS

Patients with PNH analyzed by whole-exome sequencing and mutations in *NEDD4L*

We used clinical and brain magnetic resonance imaging (MRI) data from patients with MCD referred for genetic investigations and selected 15 patient–parent trios for analysis by whole-exome sequencing. All families had a single affected patient with bilateral PNH. For the whole-exome sequencing approach, we applied a previously described experimental workflow to detect and prioritize sequence variants and validate significant findings[13,14]. We then analyzed filtered exome data and searched for recurrence of *de novo* mutations in the same gene in unrelated patients. We identified *de novo* missense changes in *NEDD4L* in two patients with bilateral contiguous PNH, bilateral syndactyly of the second and third toes, and neurodevelopmental delay (P158 and BRC217; **Fig. 1a**,**b**, **Table 1** and **Supplementary Note**). After validation of the mutations by Sanger sequencing (**Supplementary Fig. 1a**,**b**), we screened *NEDD4L* (coding exons and their flanking sequences) in a cohort of 96 patients with MCD and identified the c.2677G>A mutation (already detected in BRC217) in one additional patient (P347; **Fig. 1c**, **Table 1** and **Supplementary Fig. 1c**). Interestingly, the phenotype of this patient was also characterized by bilateral PNH, bilateral syndactyly of the second and third toes, and neurodevelopmental delay (**Table 1** and **Supplementary Note**). As the family of patient P347 consisted of two affected children (P347 and her brother), a healthy girl and healthy parents (**Supplementary Fig. 1c**), we tested the segregation of the variant in all members of the family. We found the variant to be present in a heterozygous state in the affected brother but absent from the DNA of the healthy sister and father. For the mother, however, sequencing traces consistently showed an imbalance in the height of the peaks corresponding to normal and variant alleles (**Supplementary Fig. 1c**). Altogether, these results were suggestive of germline and somatic mosaicism of a *NEDD4L* variant in the mother. To confirm this and evaluate the level of somatic mosaicism, we analyzed the mother's DNA by digital droplet PCR and found that the frequency of the

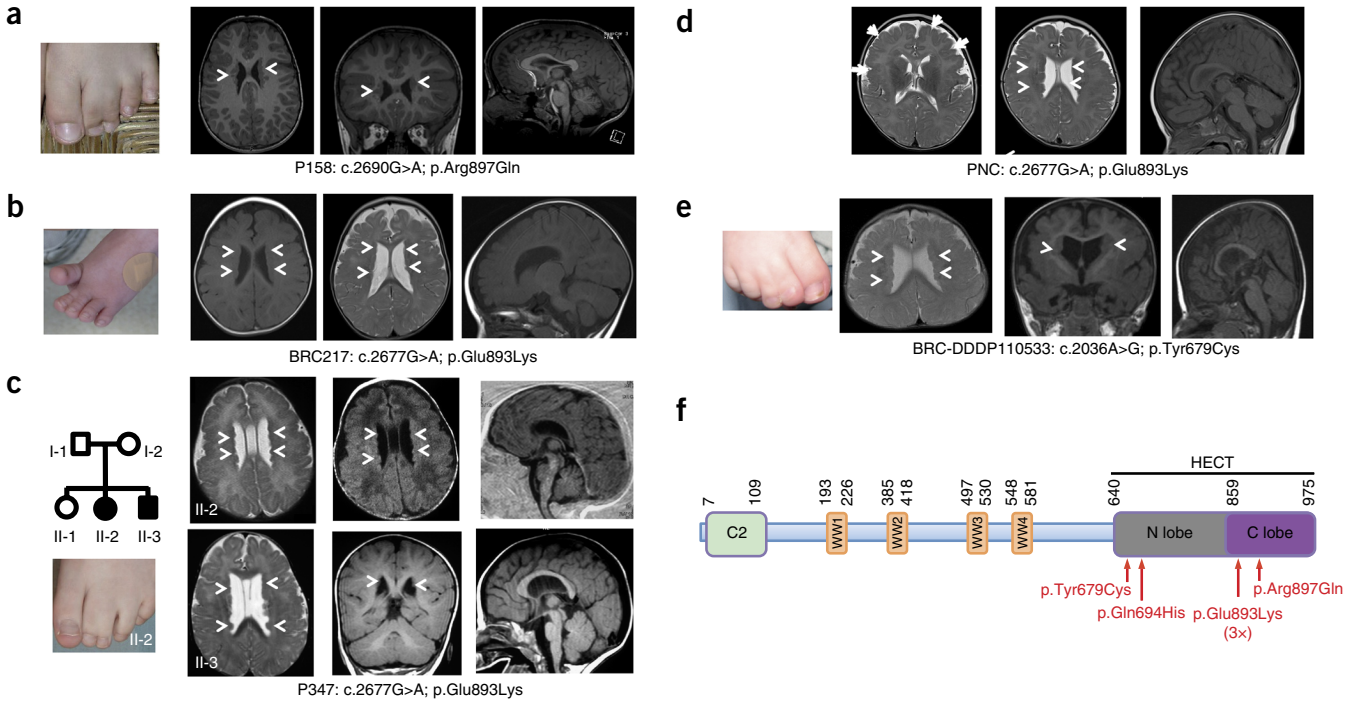

Figure 1 Mutations in *NEDD4L* cause PNH and syndactyly. (**a**–**e**) Photographs and representative sections of brain MRIs for affected individuals illustrating frequent toe syndactyly and constant PNH. For each patient, two axial sections, or one axial and one coronal section, show confluent nodules of heterotopia lining the lateral ventricles (arrowheads). Sagittal sections show thin (**c**) or dysmorphic (**a** and **c**, II-3) corpus callosum. In **d**, in addition to PNH (arrowheads), the MRI section shows frontal PMG (white arrows). MRIs were performed at the age of 8 years (**a**), 12 months (**b**), 9 and 12 months (**c**), 7 months (**d**) and 8 months (**e**). MRIs were not available for patient Pnh31124 with the c.2082G>T; p.Gln694His mutation. Written consent was obtained to publish patient photographs. (**f**) Linear representation of the NEDD4L polypeptide showing the positions in the HECT domain of the heterozygous PNH-associated mutations. NEDD4L protein is characterized by an N-terminal C2 domain known to bind Ca^{2+} and phospholipids[17], two to four WW protein–protein interaction domains[16] responsible for recognition of the substrate, and the C-terminal catalytic HECT domain[18].

Table 1 Summary of clinical and neuroimaging features of patients harboring *NEDD4L* mutations

Patients with PNH	P158 c.2690G>A p. Arg897Gln	P347 c.2677G>A p.Glu893Lys P347-II.2	P347-II.3	BRC217 c.2677G>A p.Glu893Lys	PNC c.2677G>A p.Glu893Lys	Pnh31124 c.2082G>T p.Gln694His	DDDP110533 c.2036A>G Tyr679Cys
Inheritance	*De novo*	Maternal mosaicism	Maternal mosaicism	*De novo*	*De novo*	*De novo*	*De novo*
Sex	M	F	M	F	F	F	M
Birth (GW)	40	41	41	41	38	Full term	40
Birth weight	3,750	3,160	NA	3,120	3,360	NA	3,000
Syndactyly	+	+	+	+	–	+	+
Hypotonia	+ (at birth)	NA	NA	++ (at 2 months)	+ (axial hypotonia at 34 months)	+	+ (unable to sit or walk at 6 years)
Cleft palate	–	+	Bifid uvula	+	+	+	+ (with micrognathia)
Age at last examination	6 years	12 years	2 years	4 months	4 years	8 months	6.2 years
HC (cm)	54 (+1.5 s.d.)	50 (–2.4 s.d.)	49.8 (+0.7 s.d.)	39 (–1.2 s.d.)	48 (–1.2 s.d.)	43 (–1 s.d.)	49.7(–2.32 s.d.)
Height (cm)	1.08 (–1.5 s.d.)	125 (–3.5 s.d.)	88 (+0.8 s.d.)	61 (M)	100 (+2 s.d.)	68 (–0.5 s.d.)	NA
Weight (kg)	16.5 (–1.5 s.d.)	25 (–2.5 s.d.)	10.9 (+0.7 s.d.)	5.29 (–1.1 s.d.)	14 (–0.8 s.d.)	7.6 (–2 s.d.)	20 (–0.51 s.d.)
Developmental delay	+	+ (severe)	+ (severe)	+	+	+	+ (severe)
Seizures	–	+ (late onset)	+	–	–	+ (IS at 5 months)	+
Brain MRI findings	At 8 years	At 9 months	At 2 months	At 12 months	At 7 months	At 8 months	At 8 months
PNH	+ (bilateral)	+ (bilateral)	+ (bilateral)	+ (bilateral)	+ (bilateral)	+ (bilateral)	+ (bilateral)
CC anomalies	–	–	–	Dysmorphic	Dysmorphic	–	–
Cortex anomalies	–	Cerebral atrophy	–	Frontal cortical dysplasia	PMG	–	–
Cerebellum anomalies	–	–	–	–	–	–	–
Other	Myopia	Optic atrophy Hearing impairment	Convergent Strabismus cryptorchidism	Hearing impairment,	Dysmorphic features	Abnormal visual evoked potentials, optic nerve pallor	Arthrogyposis, cryptorchidism, ptosis, complex strabismus

PNH, periventricular nodular heterotopia; PMG, polymycrogyria; CC, corpus callosum; GW, gestational week; HC, head circumference; IS, infantile spasm; NA, not available; +, present; –, absent. Transcript NM_001144967.2 (ENST00000400345) and protein Q96PU5 were used for annotation of nucleotide and protein changes, respectively.

mutated allele was around 16% (**Supplementary Table 1**). In view of these molecular data, the mother was reexamined and neurological, cognitive and behavioral evaluations were found to be normal.

Shortly after these initial findings, we reinforced the implication of *NEDD4L* by the identification of additional *de novo* mutations in three unrelated patients with PNH (**Table 1**). The first patient (PNC: **Fig. 1d**, **Table 1** and **Supplementary Fig. 1d**) was identified through targeted screening of an MCD-related panel of genes in which we included *NEDD4L*. The second and third patients—DDDP110533 (**Fig. 1e**, **Table 1** and **Supplementary Fig. 1e**) and Pnh31124 (**Table 1** and **Supplementary Fig. 1f**)—were identified through data sharing of trios exome sequenced and analyzed as part of the Deciphering Developmental Disorders and Epi4K Consortium studies. For all three patients, brain MRI results also showed the presence of PNH associated with syndactyly and neurodevelopmental delay (**Fig. 1d**,**e**, **Table 1** and **Supplementary Note**).

NEDD4L[15] (also known as *NEDD4-2*) encodes a member of the NEDD4 family of HECT-type E3 ubiquitin ligases known to regulate the turnover and function of a number of proteins involved in fundamental cellular pathways and processes[16–19]. Interestingly, all mutations associated with PNH mapped to the HECT domain (**Fig. 1f**), and relevance of their pathogenic effect was suggested by the high degree of conservation of the affected residues (**Supplementary Fig. 2a**), bioinformatics predictions (from the MutationTester tool) and structural modeling of the HECT domain (**Supplementary Fig. 2b–j**).

Functional effects of wild-type *NEDD4L* and *NEDD4L* mutants

We first analyzed the expression of *Nedd4l* during mouse brain development. As illustrated in **Supplementary Figure 3a** (*in situ* hybridization at embryonic day (E) 15), *Nedd4l* transcripts were homogenously distributed in the cortical plate, ventricular zone and ganglionic eminences. Moreover, analysis of *Nedd4l* expression by real-time qPCR in developing mouse cortex from E12.5 to E18.5 showed a peak of expression at E16.5 (**Supplementary Fig. 3b**), a developmental stage characterized by both proliferation and migration.

To assess the cellular consequences of PNH-related mutations, we transfected N2A cells with cDNA constructs for wild-type NEDD4L and three different mutants and compared expression levels and localization by immunofluorescence (**Fig. 2**). We found that wild-type NEDD4L was highly expressed (**Fig. 2a** and **Supplementary Fig. 4**), and its localization was in line with what was previously reported[20]. In contrast, PNH-related mutant proteins were hardly detectable. Indeed, 48 h after transfection, we only detected a faint signal, comparable to the background signal of cells transfected with control empty vector (**Fig. 2a**). Similar results were observed upon transfection of primary cultured mouse neurons (**Supplementary Fig. 4**). We also confirmed the lack of mutant NEDD4L expression by immunoblotting using protein extracts from transfected N2A cells (**Fig. 2b**). In view of these results, we hypothesized that PNH-associated mutants are unstable and examined NEDD4L protein expression in transfected cells treated with the proteasome inhibitor MG132. We observed by immunofluorescence and immunoblot experiments high levels of expression of PNH-related NEDD4L mutants (**Fig. 2a**,**b**).

To further ascertain that the instability of NEDD4L mutant proteins represents a disease-relevant phenotype, we tested the expression of three control variants reported in the ClinVar and/or Exome Aggregation Consortium (ExAC) databases. Referring to NM_001144967, these variants are c.698C>T, p.Ser233Leu; c.535T>A, p.Ser179Thr and c.2614G>A, p.Gly872Ser (located in the HECT domain). Cellular localization and expression levels for the different control versions of NEDD4L constructs were similar to those of wild-type NEDD4L (**Supplementary Fig. 5a**,**b**).

To strengthen the implication of a post-transcriptional mechanism, we analyzed the expression of *NEDD4L* transcripts by qRT–PCR using

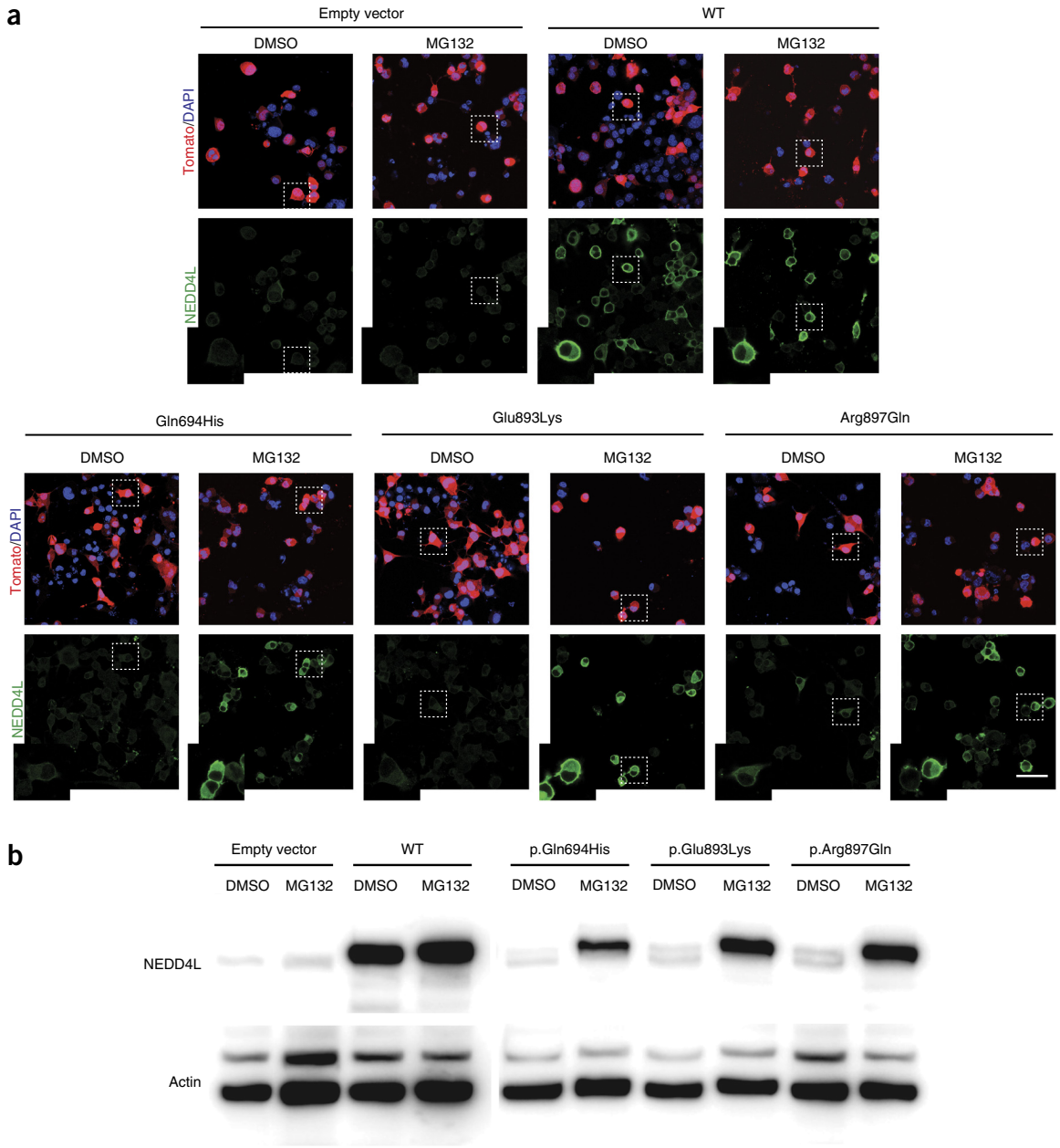

Figure 2 Expression and cellular localization of wild-type and mutant NEDD4L. (**a**) Tomato/DAPI and NEDD4L detection in N2A cells transfected with empty vector or cDNA constructs encoding wild-type (WT) or mutant NEDD4L. For each construct, cultured cells were treated with either DMSO or MG132. NEDD4L immunostaining shows a cytoplasmic distribution with enrichment in the periphery of N2A cells for wild-type NEDD4L, whereas the Gln694His, Glu893Lys and Arg897Gln mutants are not detectable. Scale bar, 50 μm. (**b**) Immunoblots using protein extracts from N2A cells transfected with constructs encoding wild-type and mutant NEDD4L and cultured in the presence of either DMSO or MG132. Blots show lack of expression of PNH-associated mutants, while transfection for wild-type NEDD4L led to a high level of expression for NEDD4L protein. Note that PNH-associated NEDD4L mutants become detectable upon treatment of N2A cells with MG132.

cotransfected reporter GFP as a normalizer. We found that wild-type *NEDD4L* transcript levels were approximately 1.5- to 2-fold higher than mutant levels (**Supplementary Fig. 6**), a range of difference that does not explain the almost complete absence of the mutant proteins.

Because all the mutations map to the catalytic HECT domain of the NEDD4L E3 ligase and lead to protein instability, we sought to assess the consequences of disease-causing variants for enzymatic activity and self-ubiquitination. To this end, we focused on the Arg897Gln mutant and compared by two different approaches the ubiquitination ability of wild-type NEDD4L and the mutant.

First, to test specifically for NEDD4L ubiquitination, we transfected N2A cells with cDNA constructs encoding N-terminally V5-tagged NEDD4L, immunoprecipitated NEDD4L from lysates using antibody to V5 and immunoblotted with an antibody to ubiquitin to detect conjugation of ubiquitin. Long exposure times for the immunoblots showed a high-molecular-mass smear mainly representing self-ubiquitinated wild-type and mutant NEDD4L. Interestingly, despite the instability of the V5-tagged mutant protein and its low amount, the intensity of the smear detected by antibody to ubiquitin was comparable to that for the wild-type protein (**Supplementary Fig. 7a**).

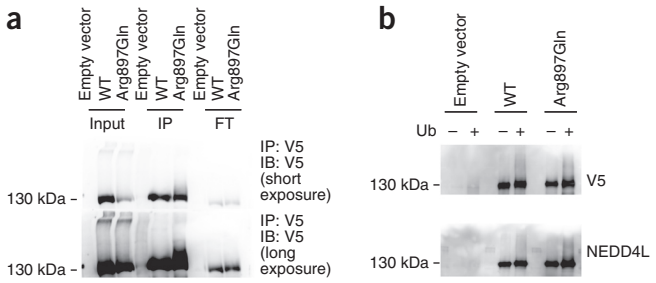

Figure 3 Ubiquitination activity of mutant NEDD4L. (**a**) Immunoprecipitation assay (IP; using antibody to V5 to precipitate tagged NEDD4L), with precipitates analyzed by immunoblot (IB) using antibodies to ubiquitin and V5 to detect ubiquitinated NEDD4L (FT, flow through). (**b**) Analysis of NEDD4L ubiquitination activity in an *in vitro* assay using wild-type and mutant NEDD4L immunopurified from the lysates of transfected N2A cells and incubated with ATP, E1 enzyme and E2 (UbcH7) enzyme with (+) or without (–) ubiquitin (Ub). Reaction mixtures were analyzed by immunoblotting with antibodies to V5 and NEDD4L. Note that, because of the instability of mutant NEDD4L and the resulting imbalance in the amounts of wild-type and mutant NEDD4L and corresponding immunoblot signals, as shown in **Supplementary Figure 7**, immunoblot analysis was performed using four times less reaction mixture for wild-type NEDD4L than for mutant NEDD4L.

Second, we compared the ubiquitination ability of immunopurified V5-tagged NEDD4L (wild type and mutant) in an *in vitro* assay using recombinant E1 and E2 (UbcH7) enzymes with or without ubiquitin. In the presence of ubiquitin, both wild-type and mutant NEDD4L exhibited ubiquitination activity as illustrated by the high-molecular-mass smear detected by antibody to NEDD4L (**Supplementary Fig. 7b**).

To further confirm and better visualize the ubiquitination activity of the NEDD4L mutant, we performed another series of immunoprecipitation and *in vitro* assays and immunoblot analysis in which we loaded four times less protein products to the assay with wild-type NEDD4L than to the one with mutant NEDD4L (**Fig. 3**). Although accurate comparison of wild-type and mutant NEDD4L ubiquitination activities is difficult, both immunoprecipitation (**Fig. 3a**) and *in vitro* ubiquitination (**Fig. 3b**) approaches showed that mutant NEDD4L induced a high-molecular-mass smear detected with antibodies to V5 and NEDD4L.

These results suggest that the ubiquitination activity of mutant NEDD4L is preserved and possibly enhanced if we take into account the substantial level of ubiquitination activity despite the instability of the protein.

At first sight, the fact that PNH-related NEDD4L mutants are unstable led us to consider a haploinsufficiency mechanism. However, previously reported findings and our data made this hypothesis questionable. For instance, postmitotic neurons deficient for both *Nedd4-1* and *Nedd4l* (analyzed in conditional double-knockout mice) migrate properly to the cortical plate[21]. Also, neuronal migration disorders and PNH are not among the features associated with haploinsufficiency resulting from heterozygous copy number variations (CNVs) reported in DECIPHER databases. Moreover, one stop-gain and three frameshift mutations were reported in the ExAC data set from which individuals affected by severe pediatric disease have been excluded. Finally, we used an *in utero* RNA interference

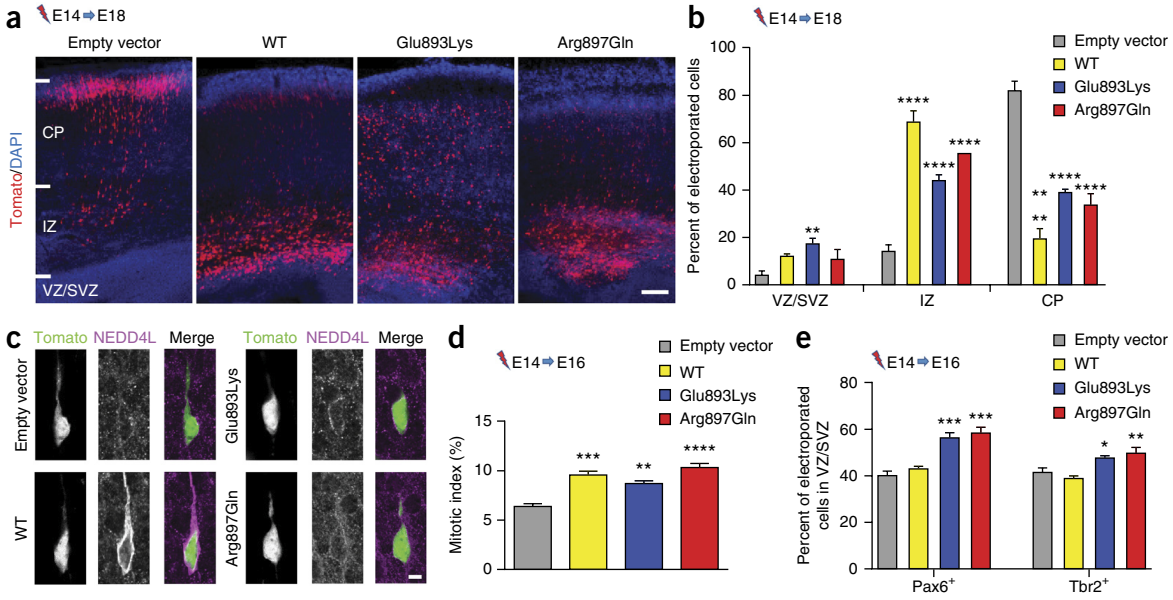

Figure 4 Effect of wild-type and mutant NEDD4L on neuronal position and progenitor proliferation. (**a**) Coronal sections of mouse brains at E18.5, 4 d after IUEP with empty vector, wild-type NEDD4L or mutant NEDD4L constructs in combination with a Tomato reporter construct. CP, cortical plate; IZ, intermediate zone; VZ/SVZ, ventricular zone/subventricular zone. Scale bar, 100 μm. (**b**) Fluorescent neurons were quantified in the regions highlighted in **a**: VZ/SVZ: empty vector (EV) vs. Glu893Lys, $P = 0.0078$; IZ: EV vs. WT, $P < 0.0001$, EV vs. Glu893Lys, $P < 0.0001$, EV vs. Arg897Gln, $P < 0.0001$; CP: EV vs. WT, $P < 0.0001$, EV vs. Glu893Lys, $P < 0.0001$, EV vs. Arg897Gln, $P < 0.0001$. Bars represent the means of fluorescent neurons ± s.e.m. of independent brains (EV, $n = 4$; WT, $n = 3$; Glu893Lys, $n = 4$; Arg897Gln, $n = 3$). (**c**) Immunofluorescence staining of NEDD4L in Tomato-positive neurons in the intermediate zone of E18.5 brains electroporated at E14.5 with NEDD4L constructs. Scale bar, 5 μm. (**d**) Percentage of electroporated neurons positive for the PH3 marker against all electroporated cells (mitotic index) in the ventricular zone as in **a** (**Supplementary Fig. 9d**): EV vs. WT, $P < 0.0001$, EV vs. Glu893Lys, $P = 0.0021$, EV vs. Arg897Gln, $P = 0.0001$. Numbers of analyzed brains are as follows: EV, $n = 4$; WT, $n = 3$; Glu893Lys, $n = 4$; Arg897Gln, $n = 3$). Error bars, s.e.m. (**e**) Quantification of Pax6$^+$Tomato$^+$ and Tbr2$^+$Tomato$^+$ cells in the ventricular zone/subventricular zone as in **a** (**Supplementary Fig. 9e**) 2 d after electroporation at E14.5: Pax6: EV vs. Glu893Lys, $P = 0.0003$, EV vs. Arg897Gln, $P = 0.0001$; Tbr2: EV vs. Glu893Lys, $P = 0.0147$, EV vs. Arg897Gln, $P = 0.0014$ (EV, $n = 4$; WT, $n = 3$; Glu893Lys, $n = 4$; Arg897Gln, $n = 3$). Error bars, s.e.m. $^*P \leq 0.05$, $^{**}P \leq 0.01$, $^{***}P \leq 0.001$, $^{****}P \leq 0.0001$.

approach to analyze the consequences of *Nedd4l* downregulation on cortical neuronal migration in mice and found no significant difference between embryo brains transfected with short hairpin RNA (shRNA) targeting *Nedd4l* and scrambled shRNA control (**Supplementary Fig. 8a**,**b**).

In view of these convergent arguments, we then sought to study the consequences of PNH-related mutations for neurodevelopmental processes. We used an *in utero* electroporation (IUEP) approach and compared the consequences of expression of wild-type NEDD4L and mutants (Glu893Lys and Arg897Gln) for neuronal positioning, neuronal progenitor proliferation and terminal translocation. To assess effects on projection neuron positioning, we electroporated *NEDD4L* constructs in combination with Tomato reporter construct into progenitor cells located in the ventricular zone of E14.5 mouse neocortices and analyzed embryo brains 4 d later (E18.5). In E18.5 brain sections, we observed that neurons electroporated with the empty vector reached the cortical plate (**Fig. 4a**,**b**). However, IUEP of wild-type NEDD4L and PNH-related mutants induced significant arrest of cells within the ventricular zone and subventricular zone and intermediate zone with corresponding depletion in the cortical plate (**Fig. 4a**,**b**). We also assessed the effect on neuron positioning at postnatal day (P) 2 and highlighted differences that paralleled those observed at E18.5. Whereas neurons electroporated with empty vector were mainly located in superficial layers II–IV of the cortical plate, we found that neurons electroporated with constructs for wild-type NEDD4L and PNH-related mutants were abnormally distributed in the white matter and in layers V and VI of the cortical plate (**Supplementary Fig. 9a**,**b**).

As our cellular data suggested that PNH-related NEDD4L mutants are unstable, we also assessed whether the same effect could be observed *in vivo* in electroporated migrating neuronal cells. We found that cells electroporated with construct for wild-type NEDD4L exhibited strong cytoplasmic immunolabeling (**Fig. 4c** and **Supplementary Fig. 9c**), consistent with a high level of NEDD4L expression. However, in neurons electroporated with mutant constructs, we only detected a faint signal that could correspond to endogenously expressed NEDD4L (**Fig. 4c** and **Supplementary Fig. 9c**).

To study terminal translocation[22–25], we conducted IUEP of the different constructs at E14.5 and collected brains 6 d later (P2) from the pups. We then assessed the distribution of electroporated neurons with a leading process adhering to the extracellular matrix (ECM) in the region previously defined as the primitive cortical zone (PCZ)[24], and in the upper and lower Cux1 regions corresponding to two equal parts of the remaining Cux1-positive layer (**Supplementary Fig. 10**). We found that expression of wild-type and mutant NEDD4L led to an abnormal distribution of neuronal cells with a deviating enrichment in the lower Cux1 region (**Supplementary Fig. 10**), suggesting that terminal translocation was disrupted.

To test the consequences of the *NEDD4L* mutations on apical and basal progenitor proliferation, we performed IUEP at E14.5 and collected embryos 48 h later for immunohistochemistry using antibodies against PH3, Pax6, Tbr2 and Ki67. We found a significantly higher percentage of Tomato-positive and PH3-positive co-labeled cells expressing wild-type protein or HECT-domain mutants in the ventricular zone when compared to Tomato-positive cells expressing the control empty vector (**Fig. 4d** and **Supplementary Fig. 9d**). These results suggested an increased mitotic index of apical progenitors electroporated with wild-type NEDD4L and PNH-related mutants. We also quantified electroporated Pax6-positive and Tbr2-positive cells in the ventricular zone and subventricular zone and found an increased number of these cell populations only in brains electroporated with PNH-related mutant constructs (**Fig. 4e** and **Supplementary Fig. 9e**).

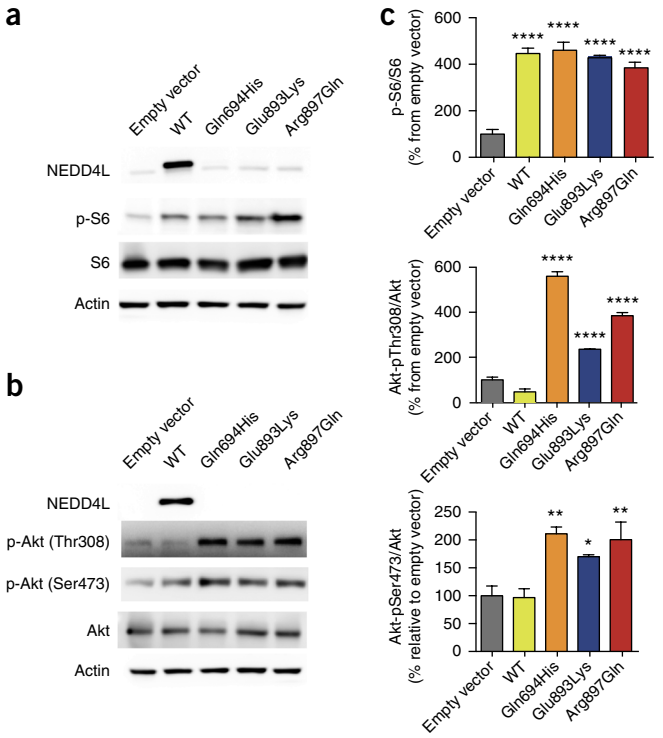

Figure 5 Wild-type NEDD4L and PNH-related mutants induce deregulation of mTORC1 and AKT activities. (**a**,**b**) Representative immunoblots using protein extracts from N2A cells transfected with empty vector or constructs for wild-type and mutant NEDD4L, showing the effect of wild-type and mutant NEDD4L on the levels of phosphorylated S6 (p-S6; reflecting mTORC1 activity) (**a**) and phosphorylated Akt (p-Akt; Thr308/Ser473) (**b**). (**c**) Histograms of densitometric measurements illustrating S6 and Akt phosphorylation. Data represent means ± s.e.m. from three independent experiments (Online Methods and **Supplementary Table 2**). $^{*}P \leq 0.05$, $^{**}P \leq 0.01$, $^{***}P \leq 0.001$, $^{****}P \leq 0.0001$.

To assess the pool of proliferating cells, we evaluated cells positive for both Tomato and Ki67 in the ventricular zone and subventricular zone; in both regions, we did not observe any differences following electroporation with control empty vector and cDNA constructs encoding wild-type and mutant NEDD4L (**Supplementary Fig. 9f**,**g**).

We also performed immunohistochemistry against the Cux1 marker at E18.5 and observed that arrested neurons electroporated with wild-type NEDD4L or PNH-related mutants expressed Cux1, indicating that misplaced neurons in deep layers of the cortex are differentiated and fated for upper layers (**Supplementary Fig. 9h**).

Finally, we labeled brain slices (E16.5 and E18.5) with antibody to cleaved caspase-3 to evaluate cell death rate and found no difference following electroporation with the different constructs (data not shown).

Pathways disrupted by wild-type and mutant NEDD4L causing PNH

Although the best known target of NEDD4L is the epithelial sodium channel (ENaC), shown to be involved in Liddle syndrome, a hereditary hypertension caused by elevated ENaC activity[26], compelling evidence demonstrating crucial regulatory roles of NEDD4L in developmental processes has recently emerged[19,27]. In this study, we sought to investigate the consequences of wild-type and mutant NEDD4L on mTOR-dependent pathways for the following main reasons.

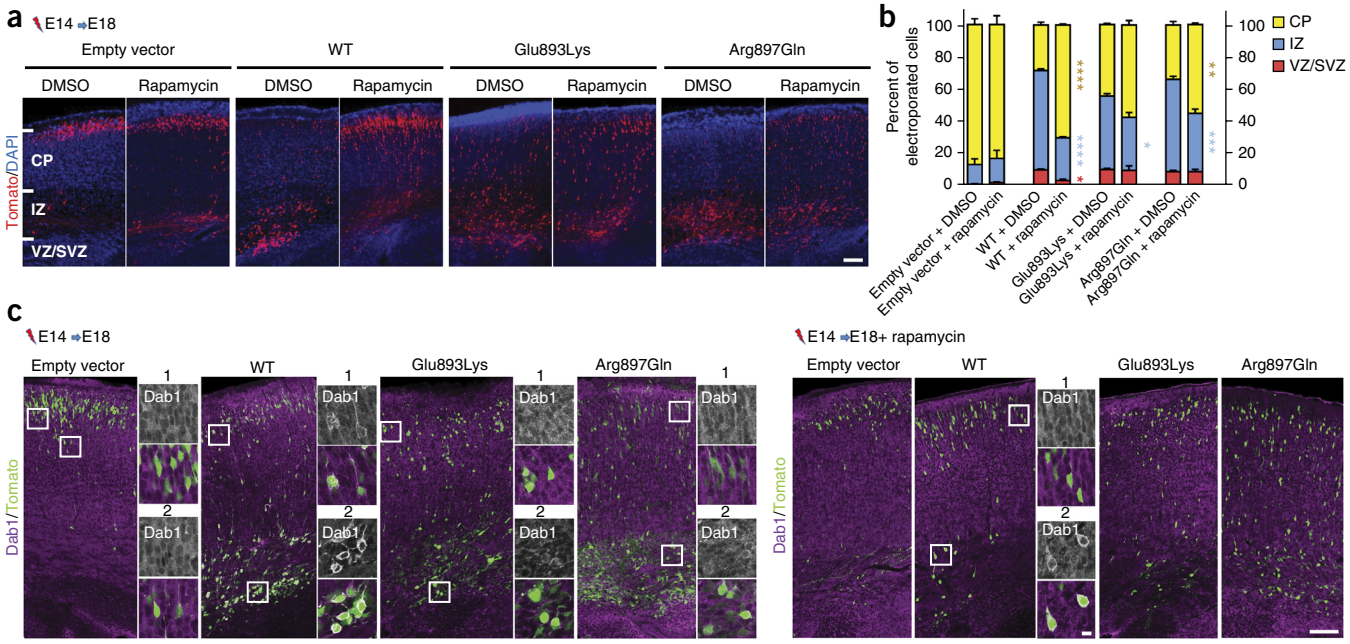

Figure 6 Effect of rapamycin treatment on neuronal positioning and Dab1 localization. (**a**) Confocal microscopy images of coronal sections from E18.5 brains electroporated at E14.5 with empty vector or constructs for wild-type and mutant NEDD4L together with a Tomato reporter vector. After IUEP, pregnant mice were treated with either vehicle (DMSO) or rapamycin (0.5 mg/kg/d). Scale bar, 100 μm. (**b**) Electroporated neurons were quantified in the regions indicated in **a**: VZ/SVZ: WT DMSO vs. WT rapamycin, $P = 0.012$, IZ: WT DMSO vs. WT rapamycin, $P < 0.0001$, Glu893Lys DMSO vs. Glu893Lys rapamycin, $P = 0.0377$, Arg897Gln DMSO vs. Arg897Gln rapamycin, $P = 0.0004$; CP: WT DMSO vs. WT rapamycin, $P < 0.0001$, Arg897Gln DMSO vs. Arg897Gln rapamycin, $P = 0.0013$. Bars represent the means of electroporated neurons in each region ± s.e.m. from three independent brains. (**c**) Immunolabeling of Dab1 on cortical slices at E18.5 from the brains of embryos subjected to DMSO or rapamycin treatment. Panels to the right of each coronal section are higher-magnification views of the regions enclosed in white boxes in the cortical plate (1) and intermediate zone (2) showing the distribution of Dab1. In arrested neurons electroporated with construct for wild-type NEDD4L from non-treated mice, note the specific pattern of Dab1 distribution and its enrichment in the periphery of the cytoplasm (mainly in arrested neurons of the intermediate zone and, to a lesser extent, neurons of the cortical plate). Scale bars, 100 μm and 10 μm (higher-magnification images). $^{*}P \leq 0.05$, $^{**}P \leq 0.01$, $^{***}P \leq 0.001$, $^{****}P \leq 0.0001$.

First, in view of the association of MCD and distal-limb abnormalities observed in patients described in this study, we wondered whether these developmental abnormalities represent a particular condition in the wide range of developmental brain and body disorders caused by dysfunctions of the interdependent phosphatidylinositol 3-kinase (PI3K)–AKT–mTOR pathways[5,14]. Second, among the many identified signaling pathways that modulate neuronal migration, the recently reported insights linking neuronal migration deficit in tuberous sclerosis complex (TSC) pathology with a cascade involving mTOR signaling, E3 ubiquitin ligase Cul5 expression and Dab1 expression[28] also led us to consider a potential effect of NEDD4L on mTOR and Dab1 signaling pathways. Third, NEDD4L was recently identified as a critical player in regulation of the crosstalk between PI3K–mTORC2 and TGF-β–activin–Smad2–Smad3 (Smad2/3) signaling pathways[29,30].

Therefore, we first tested by cellular and immunoblot assays the effect of wild-type and mutant NEDD4L on mTORC1, Akt and Smad2/3 signaling activities. Following transfection of N2A cells with constructs for wild-type NEDD4L and PNH-associated mutants, we observed an increased level of phosphorylated S6 (Ser240/Ser244) that reflects elevated mTORC1 signaling activity (**Fig. 5a,c**). In contrast, for Akt, only PNH-associated NEDD4L mutants were associated with significantly increased levels of Akt forms phosphorylated at Thr308 and Ser473 (**Fig. 5b,c**).

To reinforce the relevance and specificity of NEDD4L mutant expression to the above highlighted findings, we tested the effect of the three control variants on S6 and Akt phosphorylation and found that overexpression of the three NEDD4L variants was associated with a phosphorylation pattern that was similar to the one with wild-type NEDD4L (**Supplementary Fig. 5b**).

For Smad2/3 activity, we tested the effect of wild-type and Arg897Gln NEDD4L under the basal condition and upon activation of the TGF-β pathway by activin A on the expression levels of Smad2 phosphorylated at Ser465/Ser467, Smad3 phosphorylated at Ser423/Ser425 and Akt phosphorylated at Ser473. Under the basal condition, we found that overexpression of wild-type NEDD4L had no effect on the activation level of Smad2/3, whereas expression of mutant NEDD4L was associated with a substantial increase in the levels of phosphorylated Smad2/3 (**Supplementary Fig. 11**). Upon activation by activin A of the TGF-β pathway, we found that overexpression of wild-type NEDD4L was associated with an increase in the levels of phosphorylated Akt and Smad2/3, whereas expression of the NEDD4L mutant was associated with a substantial decrease in the levels of phosphorylated Akt and stable levels of phosphorylated Smad2/3 (**Supplementary Fig. 11**). Collectively, these results suggested that expression of the NEDD4L mutant leads to disruption of the regulated crosstalk between Akt and Smad2/3 signaling in activin–TGF-β pathways.

To assess the *in vivo* contributions of these pathways to the developmental defects described above, we used an IUEP approach in combination with treatment with rapamycin (a well-known mTORC1 inhibitor) on pregnant mice and analyzed the effect on projection neuron positioning. Interestingly, in E18.5 brain sections from embryos electroporated at E14.5 with wild-type NEDD4L and subjected to

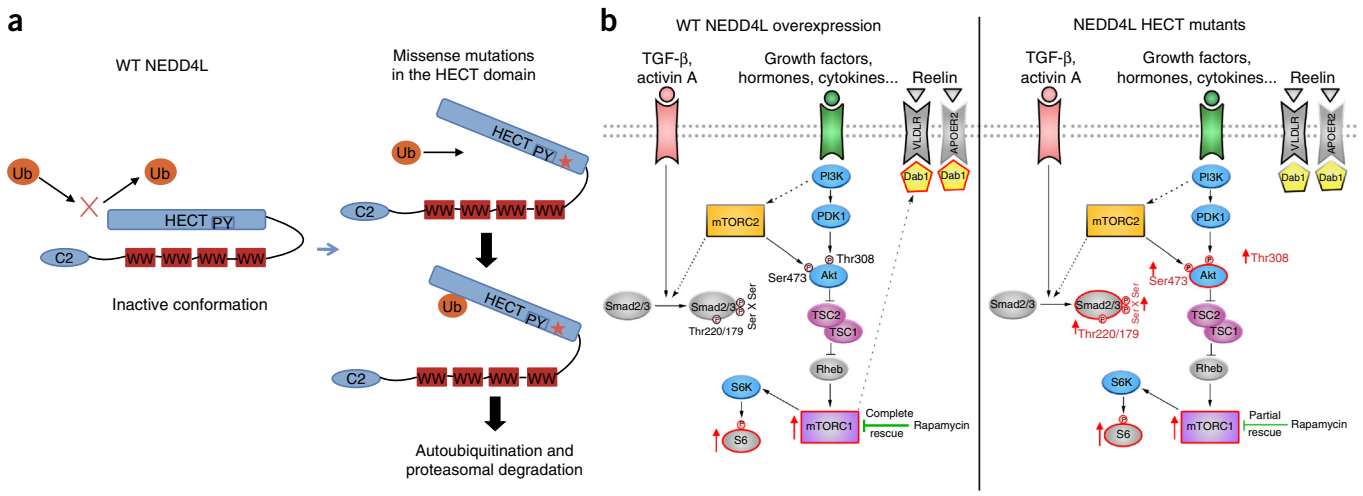

Figure 7 Models depicting the consequences of PNH-related mutations for NEDD4L stability and PI3K–Akt–mTOR and TGF-β–Smad pathways. (**a**) Wild-type NEDD4L (left) is shown in its closed and inactive conformation, and mutant NEDD4L (right) is shown with an alteration in the HECT domain predicted to lead to conformational changes that favor transition from the inactive state to the open, active state and trigger autoubiquitination and degradation. (**b**) Overview of observed deregulations under basal conditions resulting from an excess of wild-type NEDD4L (left) and expression of PNH-related NEDD4L mutants (right). Red contours indicate deregulated proteins, and dotted arrows depict indirect and poorly understood relationships between components of signaling pathways.

rapamycin treatment, we found clear rescue of the neuronal positioning defect with a distribution of electroporated cells across the cortex similar to what was observed in embryos electroporated with control empty vector (**Fig. 6a**,**b**). For this latter condition, the distribution of neuronal cells with or without rapamycin treatment was similar (**Fig. 6a**,**b**). However, rapamycin treatment induced only a partial rescue of the neuronal position defect resulting from IUEP with constructs for PNH-related mutants (**Fig. 6a**,**b**). We found that the number of Tomato-positive neurons with delayed migration was reduced in the intermediate zone, while the number of neurons that reached the cortical plate was significantly increased (**Fig. 6a**,**b**). We also analyzed the expression of NEDD4L in neuronal cells that reached the cortical plate after rapamycin treatment and found an absence of NEDD4L expression in neurons electroporated with constructs for PNH-associated mutants (data not shown), whereas neurons electroporated with construct for wild-type NEDD4L still expressed a high level of NEDD4L (**Supplementary Fig. 12**).

We then analyzed brain sections by immunohistochemistry using antibodies against Dab1 and assessed whether rapamycin-rescued neuronal position correlates with relevant changes in Dab1 expression and distribution in electroporated neurons. In arrested neuronal cells electroporated with construct for wild-type NEDD4L, we found striking labeling suggesting enrichment and nearly exclusive localization of Dab1 in the periphery of the cytoplasm, a distribution that is easily distinguishable from the diffuse pattern found in neurons electroporated with empty vector or mutant constructs (**Fig. 6c**). Interestingly, following rapamycin treatment, in the predominant pool of neurons that reached the cortical plate and that still expressed a high level of wild-type NEDD4L, we found restoration of the diffuse pattern of Dab1 localization (**Fig. 6c**). However, in neurons electroporated with constructs for PNH-associated mutants, no significant change in Dab1 cellular localization was observed, either in misplaced neurons or in the rescued neurons that reached the cortical plate (**Fig. 6c**).

DISCUSSION

Our findings demonstrate the critical role of NEDD4L in the regulation of processes involved in cortex development and implicate mutations in the HECT domain of *NEDD4L* in PNH. We report the identification of one transmitted and five *de novo* mutations in seven patients (two siblings and five unrelated patients) with a common distinguishable phenotype characterized by PNH, intellectual disability, cleft palate and syndactyly (in six of seven patients). All mutations associated with this phenotype are located in the region of *NEDD4L* encoding the HECT domain of the E3 ubiquitin ligase NEDD4L, and one of these mutations, c.2677G>A, p.Glu893Lys, is a recurrent mutation that was found in three unrelated families (**Table 1**).

One of the intriguing effects of the PNH-related mutations was the likely increase in sensitivity of the corresponding mutants to proteasome degradation. To explain this sensitivity, we propose the hypothesis illustrated by the model in **Figure 7a**. Mutations causing amino acid changes in the HECT domain could lead to conformation changes and constitutive activation of catalytic function, which in turn could trigger autoubiquitination of NEDD4L mutant variants and their degradation. This hypothesis is based on previously reported studies suggesting that catalytic activity, including autoubiquitination of HECT E3 ligases, is dependent on NEDD4L conformation[31–34].

With the model of constitutive activation due to mutations in the HECT domain, one could expect not only autoubiquitination but also aberrant ubiquitination of other NEDD4L substrates, whereas a conventional loss-of-function mechanism is expected to lead to a deficit in ubiquitination activity. Moreover, despite autoubiquitination and degradation, the predicted state of constitutive activation for NEDD4L mutants could mimic the increased activity resulting from the overexpression of wild-type NEDD4L. This model could therefore reconcile, at least partially, the apparent discrepancy regarding the observed similar neurodevelopmental defects resulting from IUEP of stable wild-type NEDD4L and the unstable NEDD4L mutants.

Another finding that was observed with wild-type and mutant NEDD4L corresponds to a positioning defect of postmitotic neuronal cells. In the misplaced neuronal cells overexpressing wild-type NEDD4L, we observed a distinct pattern of Dab1 distribution. It is worth mentioning that this finding is in line with previously reported studies that demonstrated association between excess nucleocytoplasmic Dab1 in the cytoplasm of postmitotic neurons and its inhibitory

effect on neuronal migration[35]. In arrested neuronal cells electroporated with NEDD4L mutants, the unchanged distribution of Dab1 suggests that the neuronal migration defect caused by NEDD4L mutants could be mediated by a mechanism divergent from the one disrupted by overexpression of wild-type NEDD4L. In favor of this view is evidence suggesting that excess wild-type NEDD4L is associated with the disruption of signaling pathways regulated by mTORC1 and Dab1. In contrast, PNH-related mutants might act through deregulation of mTORC1, Akt, mTORC2 and TGF-β–Smad2/3 pathway activities (**Fig. 7b**). Although further investigations are required to define the exact mechanisms by which NEDD4L overexpression and variants affect these pathways, these hypotheses are supported by a recent study showing that NEDD4L catalyzes ubiquitination of PIK3CA and regulates PI3K–AKT signaling[35] and by our rapamycin-based experiments. Indeed, the consistent rescue of the neuronal position defect and restoration of the cellular distribution of Dab1 by rapamycin treatment suggest that the migration and positioning defects induced by overexpression of wild-type NEDD4L could be mediated by mTORC1 pathway deregulation.

For PNH-related mutants, in addition to the increased activity of mTORC1, the deregulation of Akt and Smad2/3 activities under basal conditions and upon TGF-β activation provides an interesting entry point to understand further the role of NEDD4L in the regulation of neurodevelopmental processes underlying cortical development and the established implication of PI3K–AKT signaling pathways in a large spectrum of neurodevelopmental syndromes caused by activating mutations in *AKT3*, *PIK3R2* and *PIK3C*, some of which are associated with phenotypic features of MCD[5,14,36,37].

As a whole and to the best of our knowledge, we have for the first time shown that mutations in *NEDD4L* altering the HECT domain are associated with PNH and that excess NEDD4L is likely to be deleterious for brain development and functioning. This latter finding therefore provides a basis for a better understanding of phenotypes associated with duplications encompassing *NEDD4L*. In this study, we also reported evidence highlighting the disruptive consequences of *NEDD4L* mutations on the AKT–mTOR and TGF-β–Smad2/3 signaling pathways. Moreover, our study identified a potential novel disease-causing molecular mechanism, in which missense mutations might lead to a constitutively active state and loss of the mutant protein, but with functional consequences that are different from constitutive haploinsufficiency.

URLs. Exome Aggregation Consortium (ExAC), http://exac.broadinstitute.org/; MutationTester, http://www.mutationtaster.org/; DECIPHER, https://decipher.sanger.ac.uk/; Epi4K Consortium, http://www.epgp.org/; Deciphering Developmental Disorders Study, http://www.ddduk.org/; SubRVIS, http://www.subrvis.org/; Phyre web portal, http://www.sbg.bio.ic.ac.uk/phyre2/.

METHODS

Methods and any associated references are available in the online version of the paper.

Accession codes. Human *NEDD4L* (NM_001144967), mouse *Nedd4l* (NM_001114386). ClinVar accessions: SCV000267106–SCV000267109.

Note: Any Supplementary Information and Source Data files are available in the online version of the paper.

ACKNOWLEDGMENTS

We are grateful to the patients and their families for their participation. We thank D. Rotin and C. Jiang (The Hospital for Sick Children) for kindly providing humanV5-tagged Nedd4-2 constructs (pcDNA3.1-nV5 wild type, CS and Y971A constructs) and L. Lindner, M. Ruff, M. Macias and F. Francis for their thoughtful comments and help. We thank investigators from the Epi4K Consortium and the Epilepsy Phenome/Genome Project for contributing *NEDD4L*-related genotype and phenotype data. This work was supported by funding from Strasbourg University and grant ANR-10-LABX-0030-INRT, a French State Fund managed by the Agence Nationale de la Recherche under the frame program Investissements d'Avenir ANR-10-IDEX-0002-02, the Fondation pour la Recherche Médicale (FRM funding within the framework of the program Equipe FRM; J.C–DEQ20130326477), the Fondation Maladies Rares, the Fondation NRJ–Institut de France, Agence National de Recherche (ANR Blanc 1103 01, project R11039KK; ANR E-Rare-012-01, project E10107KP; ANR-13-BSV-0009-01) and European Union FP7 project GENECODYS (grant 241995) and DESIRE (grant agreement 602531), and funding provided from the National Institute of Neurological Disorders and Stroke to the Epi4k Consortium and the Epilepsy Phenome/Genome Project (NS053998, NS077364, NS077274, NS077303 and NS077276). This study was also supported in part by the NIHR Biomedical Research Centre Oxford with funding from the UK Department of Health's NIHR Biomedical Research Centre funding scheme. The views expressed in this publication are those of the authors and not necessarily those of the UK Department of Health.

AUTHOR CONTRIBUTIONS

L.B., H.J., E.L.I. and M.-V.H. conceived and designed the experiments, performed the experiments, performed statistical analysis and analyzed the data related to cellular, IUEP and functional studies. S.S. provided technical assistance and performed ubiquitination experiments. N.D. provided technical assistance, performed expression and genetic studies, and prepared reagents. J.C.-S., K.A.M., B.I., U.W.L., A.P., N.B.W., R.G., D.K., C.B., the DDD study, U.K. and N.B.-B. contributed clinical and imaging data and follow-up of patients and families. P.T. and G.M. provided assistance for IUEP studies. A.T.P., J.C.T., K.P., Y.S., N.L., G.R., B.S., A.E. and R.T. contributed to genetic studies and analysis of variants in candidate genes and screened DNA from subjects. M.M. and J.G. performed expression studies during brain development. L.N. and J.G. contributed reagents and material, as well as critical suggestions for functional studies. T.S., the DDD study, A.B., R.O., C.M., P.N. and J.-F.D. contributed to the generation of whole-exome sequencing, bioinformatics tools and analysis of sequencing data. I.S. conceived and designed ubiquitination experiments. J.C. conceived, coordinated and supervised the study, designed experiments, analyzed data and wrote the manuscript.

COMPETING FINANCIAL INTERESTS

The authors declare no competing financial interests.

1. Caviness, V.S. Jr., Takahashi, T. & Nowakowski, R.S. Numbers, time and neocortical neuronogenesis: a general developmental and evolutionary model. *Trends Neurosci.* **18**, 379–383 (1995).
2. Rakic, P. & Caviness, V.S. Jr. Cortical development: view from neurological mutants two decades later. *Neuron* **14**, 1101–1104 (1995).
3. Barkovich, A.J., Guerrini, R., Kuzniecky, R.I., Jackson, G.D. & Dobyns, W.B. A developmental and genetic classification for malformations of cortical development: update 2012. *Brain* **135**, 1348–1369 (2012).
4. Francis, F. *et al.* Human disorders of cortical development: from past to present. *Eur. J. Neurosci.* **23**, 877–893 (2006).
5. Guerrini, R. & Dobyns, W.B. Malformations of cortical development: clinical features and genetic causes. *Lancet Neurol.* **13**, 710–726 (2014).
6. Fox, J.W. *et al.* Mutations in filamin 1 prevent migration of cerebral cortical neurons in human periventricular heterotopia. *Neuron* **21**, 1315–1325 (1998).
7. Parrini, E. *et al.* Periventricular heterotopia: phenotypic heterogeneity and correlation with filamin A mutations. *Brain* **129**, 1892–1906 (2006).
8. Ferland, R.J. *et al.* Disruption of neural progenitors along the ventricular and subventricular zones in periventricular heterotopia. *Hum. Mol. Genet.* **18**, 497–516 (2009).
9. Carabalona, A. *et al.* A glial origin for periventricular nodular heterotopia caused by impaired expression of filamin-A. *Hum. Mol. Genet.* **21**, 1004–1017 (2012).
10. Lian, G. *et al.* Filamin A regulates neural progenitor proliferation and cortical size through Wee1-dependent Cdk1 phosphorylation. *J. Neurosci.* **32**, 7672–7684 (2012).
11. Sheen, V.L. *et al.* Mutations in *ARFGEF2* implicate vesicle trafficking in neural progenitor proliferation and migration in the human cerebral cortex. *Nat. Genet.* **36**, 69–76 (2004).
12. Conti, V. *et al.* Periventricular heterotopia in 6q terminal deletion syndrome: role of the *C6orf70* gene. *Brain* **136**, 3378–3394 (2013).
13. Poirier, K. *et al.* Mutations in *TUBG1*, *DYNC1H1*, *KIF5C* and *KIF2A* cause malformations of cortical development and microcephaly. *Nat. Genet.* **45**, 639–647 (2013).

14. Mirzaa, G.M. *et al.* Characterisation of mutations of the phosphoinositide-3-kinase regulatory subunit, *PIK3R2*, in perisylvian polymicrogyria: a next-generation sequencing study. *Lancet Neurol.* **14**, 1182–1195 (2015).
15. Kumar, S., Tomooka, Y. & Noda, M. Identification of a set of genes with developmentally down-regulated expression in the mouse brain. *Biochem. Biophys. Res. Commun.* **185**, 1155–1161 (1992).
16. Sudol, M., Chen, H.I., Bougeret, C., Einbond, A. & Bork, P. Characterization of a novel protein-binding module—the WW domain. *FEBS Lett.* **369**, 67–71 (1995).
17. Rizo, J. & Südhof, T.C. C2-domains, structure and function of a universal Ca^{2+}-binding domain. *J. Biol. Chem.* **273**, 15879–15882 (1998).
18. Huang, L. *et al.* Structure of an E6AP–UbcH7 complex: insights into ubiquitination by the E2–E3 enzyme cascade. *Science* **286**, 1321–1326 (1999).
19. Goel, P., Manning, J.A. & Kumar, S. NEDD4-2 (NEDD4L): the ubiquitin ligase for multiple membrane proteins. *Gene* **557**, 1–10 (2015).
20. Garrone, N.F., Blazer-Yost, B.L., Weiss, R.B., Lalouel, J.M. & Rohrwasser, A. A human polymorphism affects NEDD4L subcellular targeting by leading to two isoforms that contain or lack a C2 domain. *BMC Cell Biol.* **10**, 26 (2009).
21. Hsia, H.E. *et al.* Ubiquitin E3 ligase Nedd4-1 acts as a downstream target of PI3K/PTEN–mTORC1 signaling to promote neurite growth. *Proc. Natl. Acad. Sci. USA* **111**, 13205–13210 (2014).
22. Franco, S.J., Martinez-Garay, I., Gil-Sanz, C., Harkins-Perry, S.R. & Müller, U. Reelin regulates cadherin function via Dab1/Rap1 to control neuronal migration and lamination in the neocortex. *Neuron* **69**, 482–497 (2011).
23. Olson, E.C., Kim, S. & Walsh, C.A. Impaired neuronal positioning and dendritogenesis in the neocortex after cell-autonomous Dab1 suppression. *J. Neurosci.* **26**, 1767–1775 (2006).
24. Sekine, K., Honda, T., Kawauchi, T., Kubo, K. & Nakajima, K. The outermost region of the developing cortical plate is crucial for both the switch of the radial migration mode and the Dab1-dependent "inside-out" lamination in the neocortex. *J. Neurosci.* **31**, 9426–9439 (2011).
25. Sekine, K. *et al.* Reelin controls neuronal positioning by promoting cell-matrix adhesion via inside-out activation of integrin α5β1. *Neuron* **76**, 353–369 (2012).
26. Lifton, R.P., Gharavi, A.G. & Geller, D.S. Molecular mechanisms of human hypertension. *Cell* **104**, 545–556 (2001).
27. Boase, N.A. & Kumar, S. NEDD4: the founding member of a family of ubiquitin–protein ligases. *Gene* **557**, 113–122 (2015).
28. Moon, U.Y. *et al.* Impaired reelin-Dab1 signaling contributes to neuronal migration deficits of tuberous sclerosis complex. *Cell Rep.* **12**, 965–978 (2015).
29. Gao, S. *et al.* Ubiquitin ligase Nedd4L targets activated Smad2/3 to limit TGF-β signaling. *Mol. Cell* **36**, 457–468 (2009).
30. Yu, J.S. *et al.* PI3K/mTORC2 regulates TGF-β/activin signalling by modulating Smad2/3 activity via linker phosphorylation. *Nat. Commun.* **6**, 7212 (2015).
31. Wiesner, S. *et al.* Autoinhibition of the HECT-type ubiquitin ligase Smurf2 through its C2 domain. *Cell* **130**, 651–662 (2007).
32. Bruce, M.C. *et al.* Regulation of Nedd4-2 self-ubiquitination and stability by a PY motif located within its HECT-domain. *Biochem. J.* **415**, 155–163 (2008).
33. Wang, J. *et al.* Calcium activates Nedd4 E3 ubiquitin ligases by releasing the C2 domain–mediated auto-inhibition. *J. Biol. Chem.* **285**, 12279–12288 (2010).
34. Escobedo, A. *et al.* Structural basis of the activation and degradation mechanisms of the E3 ubiquitin ligase Nedd4L. *Structure* **22**, 1446–1457 (2014).
35. Honda, T. & Nakajima, K. Proper level of cytosolic disabled-1, which is regulated by dual nuclear translocation pathways, is important for cortical neuronal migration. *Cereb. Cortex* **26**, 3219–3236 (2016).
36. Rivière, J.B. *et al.* *De novo* germline and postzygotic mutations in *AKT3*, *PIK3R2* and *PIK3CA* cause a spectrum of related megalencephaly syndromes. *Nat. Genet.* **44**, 934–940 (2012).
37. Jansen, L.A. *et al.* PI3K/AKT pathway mutations cause a spectrum of brain malformations from megalencephaly to focal cortical dysplasia. *Brain* **138**, 1613–1628 (2015).

ONLINE METHODS

Subjects, whole-exome sequencing and variant validation. Blood or DNA samples from affected individuals and their parents and informed consent were obtained from all participants in accordance with site-specific institutional review boards. Written consent was obtained to publish patient photographs. For the selected 15 patients with PNH in association with developmental delay and/or epilepsy, 3 of the 15 patients also had PMG. For all patients, mutations in known PNH-related genes (*FLNA*, *ARFGEF2* and *C6orf70*) and pathogenic copy number variations (CNVs) had previously been excluded. DNA processing, library generation, exome enrichment and whole-exome sequencing in trios comprising affected subjects and their parents were performed and data were analyzed at the French National Centre for Genotyping (CNG, Evry, France), the Paris Descartes Bioinformatics platform and the Sanger Sequencing Centre as previously described[13,14,38]. Available genomic databases (dbSNP, 1000 Genomes Project, Exome Variant Server, Exome Aggregation Consortium and a local Paris Descartes Bioinformatics platform database) were used to filter exome variants and exclude variants with a frequency greater than 1%. *De novo* variants were analyzed by PCR and direct Sanger sequencing using DNA from patients and their parents. In the family with two affected siblings and suspected maternal somatic mosaicism, confirmation and estimation of the percentage of cells bearing the variant was performed by the droplet digital PCR approach (QX100 Droplet Digital PCR System, Bio-Rad Life Science Research) using DNA extracted from the peripheral blood of all members of the family (the two patients, the parents and the unaffected individual) and primers specific to the variant and wild-type sequences. Data were analyzed with QuantaSoft v.1.4 software (Bio-Rad Life Science Research).

Protein modeling. Amino acid substitutions were plotted onto the solved protein structure for the catalytic domain of the human NEDD4-like E3 ligase using the Phyre web portal. Models were built by homology modeling using Research Collaboratory for Structural Bioinformatics Protein Data Bank (PDB) code 2ONI. The images in **Supplementary Figure 2** were rendered using Chimera.

Cloning and plasmid constructs. Human untagged *NEDD4L* cDNA (NM_001144967.1) cloned into pCMV6-Entry vector (SC326303) was purchased from Origene. Mutations were introduced by site-directed mutagenesis using the QuikChange Site-Directed Mutagenesis kit (Agilent Technologies). Wild-type and mutated cDNAs encoding human NEDD4L were then inserted into the multiple-cloning site of psiSTRIKE vector under the control of the CAG promoter, pCDNA3-nV5. For IUEP experiments, psiSTRIKE-*NEDD4L* vectors were electroporated in combination with a pCAGGS-IRES-Tomato vector to visualize electroporated cells.

For RNA interference (RNAi) experiments, a 29-mer sequence targeting mouse *Nedd4l* mRNA and a HuSH 29-mer non-effective shRNA scrambled cassette, both commercially designed and provided by Origene in the p-GFP-V-RS vector (TG505433), were inserted into psiSTRIKE vector under the control of the U6 promoter. The *Nedd4l* shRNA directed against the coding sequence was checked for specificity in sequence databases. Because of the very low level of expression of NEDD4L, efficiency experiments were conducted using cotransfection with wild-type human *NEDD4L* cDNA and shRNA constructs in N2A cells and immunoblot analysis.

***In situ* hybridization.** Mouse *Nedd4l* sense and antisense probes (nucleotides 462 to 1,470 of transcript NM_001114386) were synthesized using T7 RNA polymerase (Roche) from pJET2.1-*Nedd4l* (nucleotides 462 to 1,470) and pJET2.1-*Nedd4l* (nucleotides 1,470 to 462) plasmids. Non-radioactive RNA *in situ* hybridization on frozen brain sections was performed as previously described[39].

qRT–PCR. Total RNA was prepared from the brains of mouse embryos at different time points of development and from cultured transfected cells with TRIzol reagent (Thermo Fisher Scientific), and cDNA samples were synthetized with SuperScript II Reverse Transcriptase (Invitrogen). qRT–PCR was performed in a LightCycler PCR instrument (Roche) using SYBR Green Master Mix (Roche). For transfection-based experiments, we used GFP as a normalizer (that is, systematically cotransfected as a reporter). For qRT–PCR of transcripts expressed from transfected cDNA constructs, RNA samples were treated with Turbo DNase (Ambion, Life Technology) to avoid amplification from plasmid DNA. Also, to ensure that we amplified transcripts expressed from transfected constructs, for each sample real-time qPCR (in triplicate) was performed using the cDNA reaction products obtained with or without reverse transcriptase and primers specific to *NEDD4L* and *GFP*.

Cell culture, transfections and immunofluorescence. Mouse neuroblastoma N2A cells were cultured in DMEM (Gibco) supplemented with 5% FCS and transfected using Lipofectamine 2000 (Invitrogen). MG132 (Calbiochem) was dissolved in DMSO solution buffer. DMSO was used as a control vehicle. Cells were treated with MG132 at a 10 μM concentration for 15 h before the end of culture. Expression of transfected genes was analyzed 48 h after transfection by immunocytochemistry and immunoblotting.

For primary cultures of neuronal cells, embryonic mouse cortical neurons (E17) were electroporated using the Amaxa mouse Nucleofector kit (Lonza) and maintained in Neurobasal medium supplemented with 2% B27, 1% glutamine and 1% penicillin-streptomycin. Cells were fixed in 4% paraformaldehyde 96 h after electroporation. Immunocytochemistry was performed according to standard procedures using antibody to Nedd4l (13690-1-AP, rabbit, Proteintech; 1:200 dilution) as the primary antibody and donkey anti-rabbit IgG 647 (A-21208, Life Technologies; 1:800 dilution) as the secondary antibody. Results were observed and photographed using a TCS SP5 confocal microscope (Leica Microsystems).

Immunoblotting. Cells were lysed in RIPA buffer (50 mM Tris-HCl, pH 7.7, 0.15 M NaCl, 1 mM EDTA and 1% Triton X-100) supplemented with protease inhibitors (Roche) and phosphatases inhibitors (Sigma-Aldrich). Protein concentration was measured using Bio-Rad protein assay reagent. Samples were denatured at 95 °C for 10 min in loading buffer and then resolved by SDS–PAGE and transferred onto nitrocellulose membranes. Membranes were blocked in 5% nonfat milk in TBS buffer with 0.1% Tween and then immunoblotted using the following primary antibodies at the specified concentrations: Nedd4l (13690-1-AP, rabbit, Proteintech; 1:1,000 dilution), actin (mouse, IGBMC; 1:1,000 dilution), Akt-pSer473 (4060, rabbit, Cell Signaling Technology; 1:1,000 dilution), Akt-pThr308 (2965, rabbit, Cell Signaling Technology; 1:1,000 dilution), Akt (pan) (4691, rabbit, Cell Signaling Technology; 1:1,000 dilution), S6-pSer236/236 (2211, rabbit, Cell Signaling Technology; 1:1,000 dilution), S6 (2217, rabbit, Cell Signaling Technology; 1:1,000 dilution), ubiquitin (sc-8017, mouse, Santa Cruz Biotechnology; 1:250 dilution) and V5 (R96025, mouse, Invitrogen; 1:5,000 dilution). All immunoblot experiments consisted of at least three independent replicates.

Immunohistochemistry. Mouse embryo brains were fixed by incubation overnight at 4 °C in 4% paraformaldehyde in 0.1 M phosphate buffer, pH 7.4. Brains were placed in a solution of 4% low-melting agarose (Bio-Rad) and cut into coronal sections (80 μm) using a vibrating-blade microtome (Leica VT1000S, Leica Microsystems). Sections were maintained in 0.01% azide in PBS buffer. For immunodetection, sections were blocked with 1× PBS with 2% normal donkey serum (Dominique Dutscher) and 0.3% Triton X-100 (PBS-T-NGS) for 30 min at room temperature. Primary antibodies were diluted in PBS-T-NGS and incubated with sections overnight at 4 °C. The following primary antibodies were used: Dab1 (AB5840, rabbit, Millipore; 1:500 dilution), Cux1 (sc-13024, rabbit, Santa Cruz Biotechnology; 1:100 dilution), Ki67 (IHC-00375, rabbit, Bethyl Laboratories; 1:250 dilution), NEDD4L (13690-1-AP, rabbit, Proteintech; 1:300 dilution), NeuN (MAB377, mouse, Millipore; 1:100 dilution), Pax6 (PRB-278P, rabbit, Covance; 1:200 dilution), PH3 (06-570, rabbit, Millipore; 1:500 dilution) and TBR2 (14-4875, rat, eBioscience; 1:200 dilution). After washes in 1× PBS, sections were incubated with Alexa Fluor–conjugated secondary antibodies (A-31573, donkey anti-rabbit IgG 647; A-21208, donkey anti-rat IgG 488; A-21206, donkey anti-rabbit IgG 488; A-31571, donkey anti-mouse IgG 647; all from Life Technologies) diluted 1:500 in PBS-T for 1.5 h at room temperature. Sections were washed and then mounted with Fluoromount-G mounting medium (Interchim). All images were acquired using a TCS SP8 confocal microscope (Leica Microsystems), and positioning analysis was achieved with ImageJ software (NIH) and proliferation analysis was performed with LAS AF software (Leica Microsystems). Graphs

were generated in GraphPad Prism 6 (GraphPad), and images were assembled with Adobe Photoshop 13.0.1 (Adobe Systems).

Ubiquitination assays. For immunoprecipitation assays, transfected cells were lysed with RIPA buffer supplemented with protease inhibitors (Roche), MG132 (25 μM) and PR-619 (20 mM) and protein extracts were incubated with anti-V5 agarose beads (A7345, Sigma) for 2 h at 4 °C under constant rotation in RIPA buffer. Immunoprecipitated proteins were eluted in Laemmli SDS buffer at 95 °C and subjected to SDS–PAGE. For *in vitro* ubiquitination assays, immunopurified NEDD4L from transfected N2A cells was incubated in reaction mixtures containing 200 nM E1 ubiquitin-activating enzyme (BostonBiochem), 400 nM E2 ubiquitin-conjugating enzyme (UbcH7; BostonBiochem), 400 μM ubiquitin (Sigma) and 2 mM ATP in reaction buffer (25 mM Tris-HCl (pH 7.5), 50 mM NaCl, 0.1 μM DTT and 4 mM $MgCl_2$). Reactions were incubated for 1 h at 30 °C and analyzed by immunoblotting with antibodies to ubiquitin, V5 and NEDD4L.

***In utero* electroporation.** *In utero* electroporation was performed as described previously[13,40] using Swiss mice (Janvier). Animal experimentations were performed at the IGBMC animal facilities. The study has Animal Experimentation Research Ethics Committee approval (2014-059). Briefly, timed pregnant mice (E14.5) were anaesthetized with isoflurane (2 l per min of oxygen, 4% isoflurane during sleep and 2% isoflurane during surgery; Minerve). The uterine horns were exposed, and a lateral ventricle of each embryo was injected using pulled-glass capillaries with Fast Green (2 μg/ml; Sigma) combined with a final concentration of 1 μg/μl of DNA constructs prepared with the EndoFree plasmid purification kit (Macherey Nagel). The expression vector pCAGGS-Tomato was systematically co-electroporated, and fluorescent Tomato protein was used to visualize electroporated cells. Plasmids were further electroporated into the neuronal progenitors adjacent to the ventricle by delivering five electric pulses at 50 V for 50 ms at 950-ms intervals using a CUY21EDIT electroporator (Sonidel). After electroporation, embryos were placed back in the abdominal cavity and development was allowed to continue until E16, E18 or P2. Embryo or pup brains were dissected and fixed in 4% paraformaldehyde in PBS overnight.

Rapamycin treatment. Rapamycin Ready-Made Solution (2.5 mg/ml in DMSO; Sigma) was previously diluted in PBS and then injected intraperitoneally at a concentration of 0.5 mg/kg daily from E15.5 to E17.5 into pregnant females electroporated at E14.5. Embryos were collected at E18.5 for analysis.

Statistics. All statistics were calculated with GraphPad Prism 6. Final counts are presented as the mean percentages ± s.e.m. One- or two-way ANOVA was performed for multiple comparisons followed by Dunnett's or Sidak's *post-hoc* tests, respectively, whereas unpaired two-tailed Student's *t* tests were used for dual comparisons. $P < 0.05$ was considered significant: $^{*}P < 0.05$, $^{**}P < 0.01$, $^{***}P < 0.001$, $^{****}P < 0.0001$. On the basis of previous IUEP experiments performed in our laboratory, we considered that at least three embryos per condition would be necessary. After histological examination, only brains with comparable electroporated regions and efficiencies were retained for quantification. Data distribution was not tested but was assumed to be normal. Blinding was not applied for data collection and analysis. Statistical details are included in **Supplementary Table 2**.

Exome sequencing data deposition. Exome sequencing data have been deposited in the database of Genotypes and Phenotypes (dbGaP) under study accession phs000653.v1.p1 for the Pnh31124 trio (proband EPGP012746) and the European Genome-phenome Archive (EGA) under accession EGAD00001001848 for the DDDP110533 trios. For the other patients analyzed by the whole-exome sequencing approach, no consent was obtained from the patients to deposit the data in a repository.

38. Wright, C.F. *et al.* Genetic diagnosis of developmental disorders in the DDD study: a scalable analysis of genome-wide research data. *Lancet* **385**, 1305–1314 (2015).
39. Cau, E., Gradwohl, G., Fode, C. & Guillemot, F. Mash1 activates a cascade of bHLH regulators in olfactory neuron progenitors. *Development* **124**, 1611–1621 (1997).
40. Kielar, M. *et al.* Mutations in *Eml1* lead to ectopic progenitors and neuronal heterotopia in mouse and human. *Nat. Neurosci.* **17**, 923–933 (2014).

doi:10.1038/ng.3676